EPJ Web of Conferences **321**, 02011 (2025) https://doi.org/10.1051/epjconf/202532102011
*APITECH-VII-2025*

# Formation of chromium–nickel steel cladding layers on petrochemical equipment components using the double-electrode surfacing method

*Sergey* Elsukov*, *Ilya* Zorin, *Vladimir* Lysak, *Valentin* Kharlamov, and *Sergey* Fastov

Volgograd State Technical University, 28, Lenin avenue, Volgograd, 400005, Russia

**Abstract.** This article discusses the results of investigating the structure of chromium–nickel metal obtained through electric arc surfacing with single and double electrodes in a protective gas. It provides recommendations for forming a defect-free cladding layer by welding with double electrodes. The results show that double electrodes can achieve comparable resistance to intergranular corrosion while reducing electrode metal consumption by approximately 30–35%. Additionally, this method results in a more technologically advanced form of deposited beads.

## 1 Introduction

During the production of vessels and equipment for petrochemical processing and storing liquefied hydrocarbon gases, surfacing steel parts with corrosion- and heat-resistant chromium–nickel austenitic steels is a critical technological operation. Among the most productive and effective methods for surfacing these materials on the internal and flange surfaces of petrochemical and oil and gas equipment (such as reactors, heat exchangers, and adsorbers) are electric arc surfacing under a flux layer [1, 2] and electroslag surfacing with strips [3, 4]. The widespread industrial application of these methods is attributed to their suitability for cladding easily accessible internal cylindrical surfaces of large diameters and areas, which are predominantly characteristic of petrochemical equipment.

However, when surfacing small-diameter internal surfaces (up to 500 mm) or flat surfaces of flanges and pipeline fittings, applying these methods becomes challenging owing to the limited sizes of the workpieces and their tendency to overheat. Therefore, there is an increasing need for technologically flexible surfacing processes, such as plasma transferred arc (PTA) welding and electric arc surfacing with consumable electrodes in shielding gases. PPS is highly efficient [5-6] for surfacing relatively thin layers (ranging from 0.5 to 4 mm) with minimal substrate melting. Additionally, the high specific melting rate of the electrode metal in the welding arc, combined with the extensive range of available welding wires, makes this method preferable for forming multilayer cladding layers (with thicknesses of 3–8 mm). However, this approach is associated with significantly increased heat input compared to plasma surfacing [7].

* Corresponding author: serzh.elsukov@yandex.ru

Therefore, current efforts are focused on minimizing the depth of melting of the workpiece, typically made of carbon steel, to reduce the dilution of the plating layer with iron from the base metal [8]. This helps maintain the necessary levels of chromium and nickel for corrosion resistance and resistance to intergranular corrosion (IGC) [9]. For instance, using pulsed arc welding allows for control of heat input into the electrode and base metal [10] and the near-weld zone [11]. However, this method does not address the low productivity issues associated with pulsed arc welding.

Technologically, one of the simplest methods for controlling heat input during multilayer surfacing is the use of double electrodes connected to a common welding current source, either with single-polarity [12] or reverse-polarity [13] connection. The effectiveness of this double-electrode process in corrosion-resistant surfacing technologies in shielding gases depends on studying the characteristics of forming the cladding layer from adjacent beads of deposited metal, as well as its structure and resistance to IGC.

The objective of this study is to improve the quality of forming cladding layers from chromium–nickel austenitic steel by employing double-electrode surfacing in argon–carbon dioxide gas mixture.

## 2 Materials and equipment

To achieve the necessary chemical composition of the corrosion-resistant metal cladding layer in accordance with regulatory requirements, surfacing is performed by incorporating a transition layer to ensure the cladding layer's resistance to IGC. This transition layer compensates for the reduced chromium and nickel content in the deposited metal caused by its dilution with the steel substrate. For this purpose, wire OK Autrod 309LSi (equivalent to Sv-07Kh25N12G2T) with a diameter of 2 mm was used at a current of $I = 330 \pm 15$ A, voltage $U_a$ = 26–27 V, and a travel speed $V_s$ = 20 cm/min. The cladding layer was deposited using wire AG ER-347Si (equivalent to Sv-08Kh19N10G2B) with a diameter of 1.6 mm, employing the following parameters: current $I = 280 \pm 15$ A, voltage $U_a$ = 25–26 V, and travel speed $V_s$ = 20 cm/min. This surfacing regime provided a heat input $q_s$ = 14–15 kJ/cm. The distance between the axes of the electrode wires was 8 mm. Equipment utilized included a thyristor rectifier LAF 1001 (ESAB) and a welding machine A6 MasterTrack (ESAB), equipped with an original gas delivery device containing a gas diffuser and a water-cooled nozzle. The gas mixture flow rate of 98% Ar + 2% $CO_2$ was maintained at 15–17 L/min.

**Table 1.** The chemical composition of the welding wires used.

| Material | Composition, [wt.%] | | | | | | | | | | | |
|---|---|---|---|---|---|---|---|---|---|---|---|---|
| | **Fe** | **C** | **Si** | **Mn** | **Ni** | **Cr** | **Ti** | **Mo** | **Nb** | **Cu** | **S** | **P** |
| Corrosion-resistant layer | | | | | | | | | | | | |
| AG ER 347Si $d_e$ = 1.6 mm | Base | ≤0.08 | 0.65–1.0 | 1–2.5 | 9–11 | 19–21 | – | ≤0.75 | 10×%C–1.00 | ≤0.75 | ≤0.02 | ≤0.03 |
| Transition layer | | | | | | | | | | | | |
| Sv-07Kh25N12G2T $d_e$ = 2.0 mm | Base | ≤0.09 | 0.3–1 | 1.5–2.5 | 11–13 | 24–26.5 | 0.6–1 | – | – | ≤0.3 | ≤0.02 | ≤0.035 |

The surfacing was performed on 8 mm thick plates fabricated from VSt3sp and 15Kh5M steels (Table 2) without preheating or accompanying heating. After surfacing the transition layer on the 15Kh5M steel plate, an intermediate heat treatment (high annealing) was performed at 700°C for 2 h.

**Table 2.** The chemical composition of plates made of steel VSt3sp GOST 380-94 and 15Kh5M GOST 20072-74.

| Material | Composition, [wt.%] | | | | | | | | | | |
|---|---|---|---|---|---|---|---|---|---|---|---|
| | Fe | C | Si | Mn | Ni | Cr | Ti | Mo | S | P | Cu |
| VSt3sp | 98 | 0.14–0.22 | 0.12–0.3 | 0.4–0.65 | ≤0.3 | ≤0.3 | – | – | ≤0.05 | ≤0.04 | ≤0.3 |
| 15Kh5M | 91 | ≤0.15 | ≤0.5 | ≤0.5 | ≤0.6 | 4.5–6 | ≤0.03 | 0.45–0.6 | ≤0.025 | ≤0.03 | ≤0.2 |

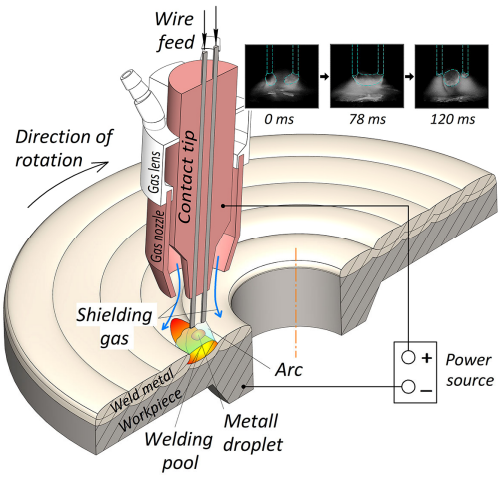


**Fig. 1.** Schematic diagram illustrating the formation of a cladding layer on the flange surface through arc welding with double electrodes.

## 3 Methods

The resistance of the deposited metal to IGC was assessed using the AMU method in accordance with GOST 6032–2017. Flat specimens measuring 120 × 20 × 5 mm were fabricated from multilayer metal deposited under comparable conditions using two technological variants (Table) and a transition layer. The samples were heated to 700°C in an aggressive environment, which is required for metal containing niobium. Subsequently, to detect IGC after testing, samples were bent at an angle of 90° ± 5° in accordance with GOST 14019.

The metal's microstructure was analyzed before and after etching using an analysis system, which included an optical microscope. Additionally, a scanning electron microscope, Phenom XL, was employed to assess contamination by non-metallic inclusions, identify structural constituents, determine the presence of defects, and analyze altered structures in the surface layers.

Micro X-ray spectral analysis was performed using the ion–electron microscope Versa 3D. Electron backscatter diffraction (EBSD) was utilized to assess the mutual arrangement and sizes of austenite grains in the structure (EDAX). X-ray phase analysis was performed using the Bruker D8 X-ray diffractometer, and phase identification was carried out using Diffrac.EVA software (version 4.2.1). The microstructure was revealed through etching with a reagent consisting of 520 mL of water, 80 mL of HF, and 400 mL of $H_2SO_4$. The hardness of the deposited metal was measured using the Rockwell method (scale B), followed by conversion of values to Brinell hardness numbers.

**Table 3.** Technological surfacing options and chemical composition of samples for testing metal susceptibility to IGC.

| Variant No. | Surfacing method | Number of layers | Composition, [wt.%] * | | | | | | | |
|---|---|---|---|---|---|---|---|---|---|---|
| | | | C | Si | Mn | Ni | Cr | Nb | Co | Ti |
| Transition layer | | | | | | | | | | |
| - | 2 electrodes | 1 | 0.12 | 0.45 | 1.02 | 7.7 | 12.5 | - | - | 0.4 |
| Corrosion-resistant layers | | | | | | | | | | |
| 1 | 2 electrodes | 2 | 0.01 | 0.7 | 1.58 | 9.25 | 18.7 | 0.22 | 0.17 | 0.1 |
| 2 | 1 electrode | 2 | 0.01 | 0.79 | 1.62 | 9.2 | 18.2 | 0.2 | 0.2 | 0.1 |

* The measurement was performed on the surface of the deposited beads.

## 4 Results and discussion

We experimentally determined that to achieve a high-quality cladding layer, it is necessary to address the formation of a defect known as an undercut during the double-electrode surfacing process. This defect occurs because the substrate of the deposited bead comprises approximately 50% of the surface of the previously deposited metal, which differs from surfacing with a single electrode. Consequently, the droplet of wire that has not yet detached from the end does not seal the weld pool but instead covers the bead's surface from a previous pass. Thus, the liquid metal from the weld pool spills off the bead, creating a local depression on its surface and disrupting the continuity of the deposited metal layer between adjacent beads. Therefore, in multipass surfacing, it is recommended to change the electrode inclination angle from the vertical axis by 2°–5° after the first pass and ensure a 30–40% overlap of the adjacent bead.

The test results showed that the deposited metal's resistance to IGC was achieved using single- and double-electrode surfacing methods. No cracks or fragmented grains were observed in the metal. Comparable results were achieved with reduced consumption of electrode metal (by 30–35%) when utilizing the double-electrode scheme for cladding layer formation. Additionally, a more technologically advanced bead shape was obtained. Thus, the required chromium (not less than 18 wt.%) and nickel (not less than 9 wt.%) contents in the second layer of deposited metal are ensured using the double-electrode method, with a height from the surface level of the base metal of approximately 7 mm (Figure 2, a). In contrast, with single-electrode surfacing, a similar content of Cr and Ni is achieved when forming a multilayer deposited metal with a height of at least 13 mm (Figure 2, b).

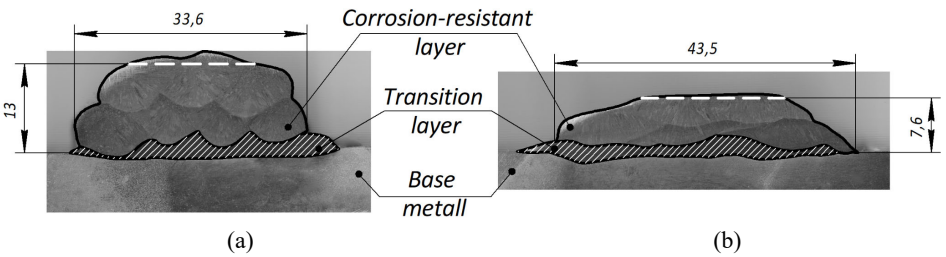


**Fig. 2.** Cross-section of metal deposited via single-electrode (*a*) and double-electrode (*b*) methods. The dashed line indicates the height of the deposited metal where comparable chromium and nickel contents are attained.

The analysis of the metal structure cross-section (Figure 3) revealed a typical dendritic structure of austenitic deposited metal crystallized by a ferritic–austenitic mechanism,

displaying a lamellar morphology of ferrite. The size of the structural components remains consistent, irrespective of the surfacing method.

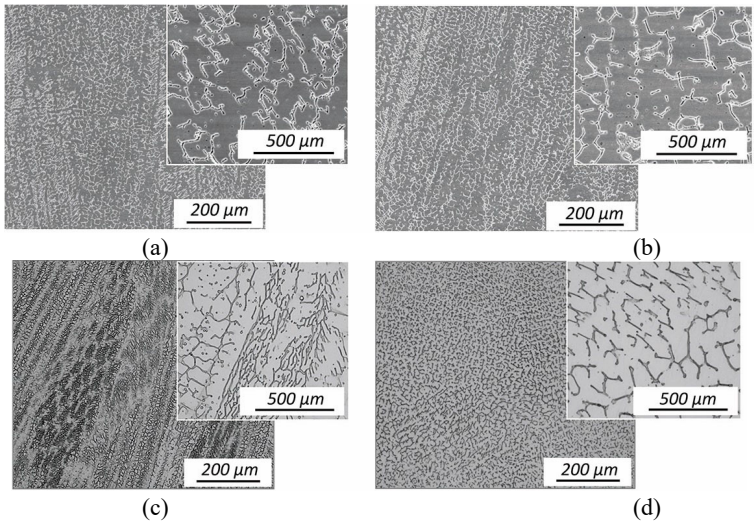


**Fig. 3.** Structures (in the second layer) of metal deposited using a double-electrode (*a, c*) and single-electrode (*b, d*) methods (*a, b* – transverse section of the deposited metal; *c, d* – longitudinal section).

However, EBSD revealed that in metal deposited using double electrodes, the size of large grains was 0.21–0.42 mm (Figure 4, a), and their structure was more dispersed. Conversely, metal deposited using the single-electrode method typically exhibits larger elongated grains with widths of 0.27–0.67 mm (Figure 4, b).

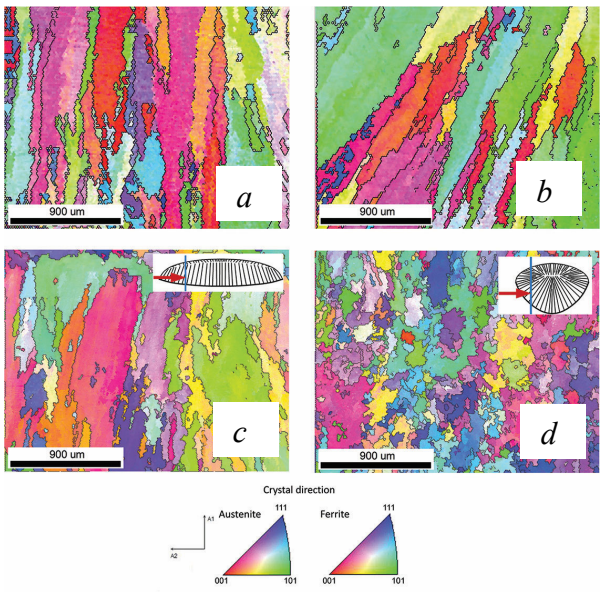


**Fig. 4.** EBSD maps in the second layer of austenitic metal deposited by double-electrode (*a*, *c*) and single-electrode (*b*, *d*) methods. The vertical line indicates the position of the cutting plane selected for studying the metal in the longitudinal section. (*a*, *b* – transverse section of the deposited metal; *c*, *d* – longitudinal section).

A different distribution pattern of grain sizes emerges when analyzing the deposited metal longitudinally. Metal deposited by the single-electrode method demonstrates the highest degree of grain refinement (Figure 4, d), with grain sizes ranging from 0.1 to 0.2 mm according to EBSD analysis. In metal deposited using double electrodes, elongated grains are prevalent (Figure 4, c), exhibiting shapes and sizes (length ~1.5 mm, width 0.2–0.5 mm) similar to those observed in the transverse section.

The differences in structure formation in two perpendicular planes are attributed to the change in the crystallization mechanism of the deposited metal when transitioning from surfacing with a single electrode to using double electrodes. In this case, the shallow depth of fusion and the nearly linear profile of the melting line, resulting from a more evenly distributed heat input widthwise across the weld pool, influence the predominantly vertical direction of crystal growth throughout the entire volume (Figure 4, *a, c*). Consequently, both in the transverse and longitudinal sections of the deposited metal, the prevailing grain orientations are (001) and (101) (Figure 4, *a, c*).

In the metal obtained using single-electrode surfacing, grain orientations (001) and (101) are predominant only when analyzing the metal in the transverse section (Figure 4, *b*). In contrast, orientation (111) is prevalent in the longitudinal section (Figure 4, *c*). This is attributed to the characteristics of single-electrode welding and surfacing processes, which involve a concave shape of the crystallization front. Consequently, the direction of crystallite growth significantly deviates from the vertical axis.

Electron microscopic investigations have revealed that the distribution of nickel, chromium, and niobium in the metal deposited by single- and double-electrode processes is nearly identical (Figure 5). Analysis of the phase composition indicates that austenite is the sole phase present in the deposited transition layer, while the structure of the cladding layer contains up to 10% of the ferritic phase (Figure 6).

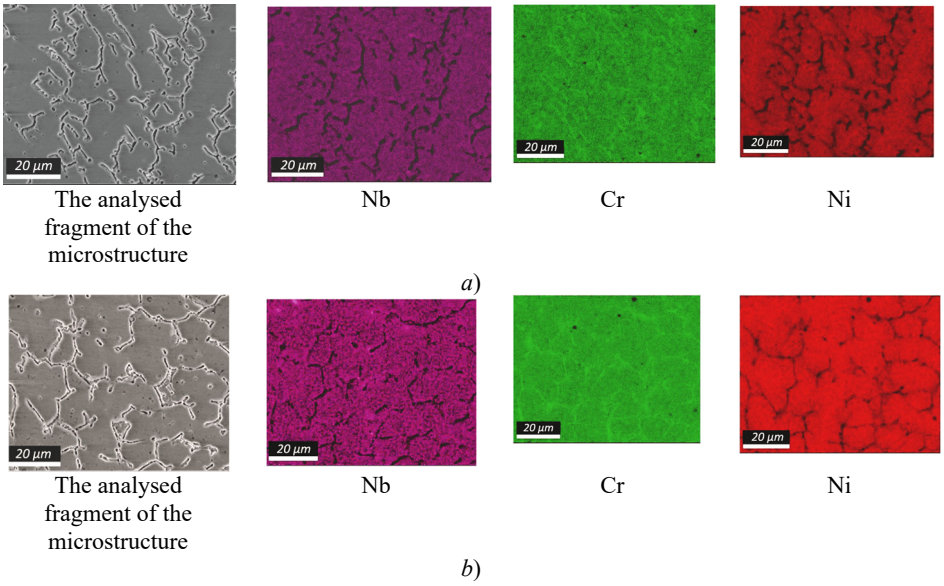


**Fig. 5.** Distribution maps of alloying elements in the second layer of metal deposited by single (a) and double electrodes (b).

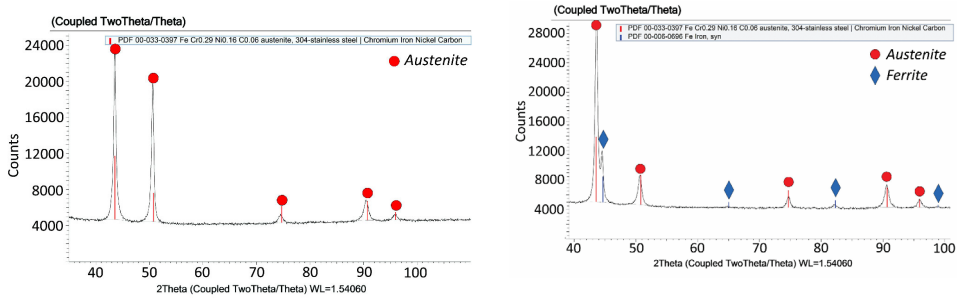


a) b)

**Fig. 6.** Diffractogram of the deposited metal in the transition (a) and cladding (b) layers (surfacing with double electrodes).

Analysis of the transition zone from the base to the deposited metal reveals the absence of carbide streaks or other diffusion and crystallization interlayers (Figure 7). Upon crossing the melting line, the metal deposited by double electrodes exhibits an increased content of nickel and chromium, indicating minimal dilution by the steel substrate.

The variation in hardness between the base metal and the deposited layers suggests that irrespective of the surfacing method, the distribution of hardness in the heat-affected zone and the transition layer of the deposited metal remains comparable. However, while the highest hardness value corresponds to the transition layer when surfacing on VSt3sp using both methods, for quenchable steel 15Kh5M, the peak values are shifted to the heat-affected zone (HAZ) (Figure 8). The obtained values fully comply with regulatory documentation requirements (the hardness value of the base metal after surfacing should not exceed 240 HB, and the hardness value of the transition and corrosion-resistant layers should be 220 HB). The slight decrease in hardness (160–170 HB) in the layer of austenitic corrosion-resistant metal deposited by the double-electrode method is attributed to a smaller proportion of perlite-type steel.

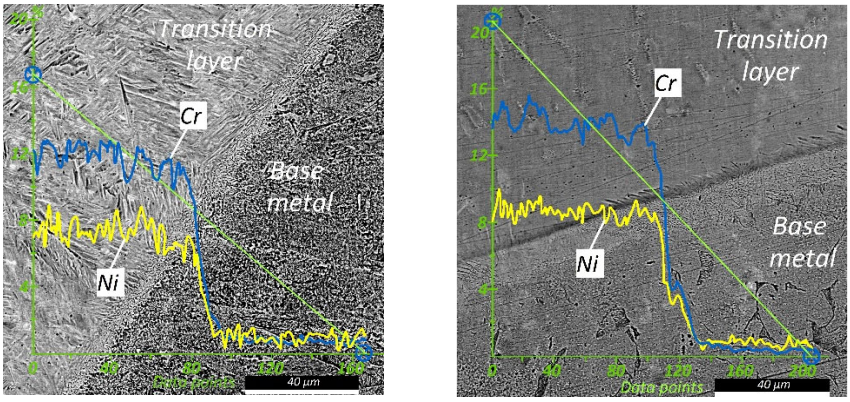


a) b)

**Fig. 7.** The distribution of chromium and nickel (cross-sectional view) in the transition layer deposited on VSt3sp steel using single (a) and double (b) electrodes.

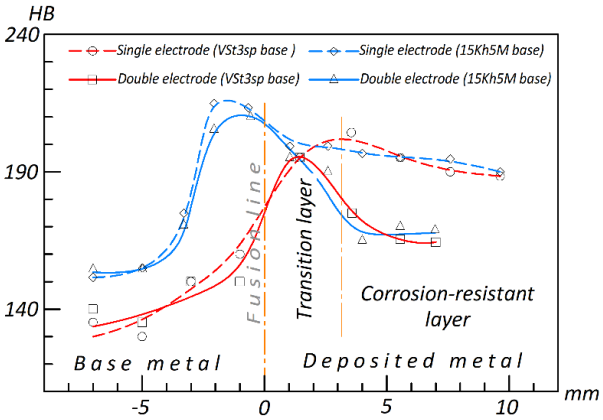


**Fig. 8.** Hardness distribution (cross-sectional view) in metal deposited on VSt3sp and 15Kh5M steel using single- and double-electrode surfacing.

Therefore, employing double-electrode surfacing in argon–carbon dioxide gas mixture enhances the efficiency of cladding with corrosion-resistant steel of horizontal and potentially cylindrical surfaces of pipeline fittings in petrochemical equipment.

## 5 Conclusion

Double-electrode surfacing yields the typical dendritic structure characteristic of austenitic deposited metal, where grains with (001) and (101) orientations are prevalent. These orientations are attributed to the altered direction of crystal growth in a wider weld pool. This method facilitates improved gas removal from the melt and reduces the tendency of austenitic metal to form pores.

Both surfacing methods achieve the resistance of the deposited metal to IGC. However, comparable results are attained when using double electrodes, with a lower consumption of electrode metal needed to form the cladding layer.

The study was supported by a grant from the Russian Science Foundation № 24-23-20068, https://rscf.ru/project/24-23-20068/ and a grant from the Volgograd Region Administration under agreement No. 7 dated May 31, 2024.

## References

1. M. Del Prete, L. Saturno, D. Quintiliani, Welding International **28(8)**, 617-628 (2014).
2. M.K. Saha, S. Das, Journal of the Association of Engineers **86(1-2)**, 51-63 (2016).
3. M. Mandina, M. Magnasco, G. Zappavigna, Welding International **28(5)**, 380-396 (2014).
4. J.V. Matias, M.J. Lourenço, J.C. Jorge, L.F.G. de Souza, H.N. Farneze, M.C. Mendes, L.S. Araujo, Journal of Materials Research and Technology **15**, 5151-5164 (2021).
5. M. Dhaneshwaran, S. Jhavar, Materials Today **46**, 1116-1121 (2021).
6. V. Balasubramanian, A.K. Lakshminarayanan, R. Varahamoorthy, S. Babu, Journal of Iron and Steel Research, International **16(1)**, 44-53 (2009).
7. P. Luchtenberg, P.T. de Campos, P. Soares, C.A.H. Laurindo, O. Maranho, R.D. Torres, Surface and Coatings Technology **375**, 688-693 (2019).

8. Y.N. Lankin, I.A. Ryabtsev, V.G. Soloviov, Y.P. Chernyak, V. Zhdanov, The Paton Welding J **9**, 25-29 (2014).
9. J. Li, H. Li, Y. Liang, P. Liu, L. Yang, Y. Wang, Corrosion Science **166**, 108445 (2020).
10. Y.N. Saraev, A.G. Lunev, V.M. Semenchuk, A.S. Nepomnyashchii, Russian physics journal **62**, 1573-1579 (2020).
11. V.A. Lebedev, Procurement production in mechanical engineering **16(10)**, 440-443 (2018).
12. S.K. Elsukov, I.V. Zorin, S.A. Fastov, V.I. Lysak, Welding and diagnostics **2**, 37-41 (2023).
13. Q. An, Y. Wen, K. Matsuda, J. Xu, D. Wu, Y. Zou, Materials Research Express **8(1)**, 016529 (2021).